



Contents lists available at ScienceDirect

Bioorganic & Medicinal Chemistry

journal homepage: www.elsevier.com/locate/bmc

Design, synthesis, and biological evaluation of dibromotyrosine analogues inspired by marine natural products as inhibitors of human prostate cancer proliferation, invasion, and migration

Asmaa A. Sallam^a, Sindhura Ramasahayam^b, Sharon A. Meyer^b, Khalid A. El Sayed^{a,*}^a Department of Basic Pharmaceutical Sciences, College of Pharmacy, University of Louisiana at Monroe, 1800 Bienville Drive, Monroe, LA 71201, USA^b Department of Toxicology, College of Pharmacy, University of Louisiana at Monroe, 1800 Bienville Drive, Monroe, LA 71201, USA

ARTICLE INFO

Article history:

Received 13 July 2010

Revised 24 August 2010

Accepted 30 August 2010

Available online 29 September 2010

Keywords:

Aeropylsinin-1

Angiogenesis

Dibromotyrosine

Invasion

Marine natural products

Migration

Proliferation

Prostate cancer

Verongiaquinol

ABSTRACT

Bioactive secondary metabolites originating from dibromotyrosine are common in marine sponges, such as sponges of the *Aplysina* species. Verongiaquinol (**1**), 3,5-dibromo-1-hydroxy-4-oxocyclohexa-2,5-diene-1-acetamide, and aeropylsinin-1 are examples of such bioactive metabolites. Previous studies have shown the potent antimicrobial as well as cytotoxic properties of verongiaquinol and the anti-angiogenic activity of aeropylsinin-1. The work presented herein shows the design and synthesis of dibromotyrosine-inspired phenolic ester and ether analogues with anti-angiogenic, anti-proliferative and anti-migratory properties and negligible cytotoxicity. Several analogues were synthesized based on docking experiments in the ATP binding site of VEGFR2 and their anti-angiogenic potential and ability to inhibit angiogenesis and prostate cancer proliferation, migration and invasion were evaluated using the chick chorioallantoic membrane (CAM) assay, MTT, wound-healing, and Cultrex[®] BME cell invasion assay models, respectively. Analogues with high docking scores showed promising anti-angiogenic activity in the CAM assay. In general, ester analogues (**5**, **6**, and **8–10**) proved to be of higher anti-migratory activity whereas ether analogues (**11–14**) showed better anti-proliferative activity. These results demonstrate the potential of dibromotyrosines as promising inhibitory scaffolds for the control of metastatic prostate cancer proliferation and migration.

© 2010 Elsevier Ltd. All rights reserved.

1. Introduction

Marine sponges are extraordinary rich sources of biologically active secondary metabolites, unrivaled by any other marine organism.¹ Brominated natural products are common in marine sponges. The ecological function of these brominated natural products is not clear yet, but they may play a role in chemical defense and deterrence.² Sponges of the *Aplysina* species are characterized by the presence of secondary metabolites that originate from dibromotyrosine,^{1–3} such as aeropylsinin-1, fistularin-3, agelorsin A and B (Supplementary data, Fig. S1), verongiaquinol (**1**), as well as many others. Many biological properties have been described for these brominated secondary metabolites including antimicrobial activity,^{4,5} cytotoxicity against several tumor cell lines,^{2,4} inhibition of the EGFR tyrosine kinase and anti-angiogenic properties,^{6–8} which renders them an interesting class for further investigation as potential anti-cancer scaffolds.

The structurally-simple dibromotyrosines, verongiaquinol and aeropylsinin-1, inspired the work presented herein. Verongiaquinol

(**1**), a 3,5-dibromo-1-hydroxy-4-oxocyclohexa-2,5-diene-1-acetamide, was shown to possess potent antimicrobial activity, against a wide range of Gram positive and negative bacteria and fungi, as well as cytotoxic properties.^{4,5} The cytotoxic effect of **1** was attributed to the formation of free radicals.² The dienone structure provides the basis for this free radical formation. Previous reports of the anti-angiogenic potential of aeropylsinin-1,^{6,8} isolated from sponges of the *Aplysina* species, encouraged the molecular modeling and docking studies of dibromotyrosines at the ATP binding site of the vascular endothelial growth factor receptor 2 (VEGFR2) as one of their possible molecular target(s) in an attempt to design and synthesize a number of analogues with improved activity and low cytotoxicity.

The role of VEGF/VEGFR axis in angiogenesis and cancer progression is well-documented.^{9–11} Angiogenesis is a tightly regulated multistep process, whereby new capillaries sprout and grow from existing blood vessels.⁹ In cancer, angiogenesis is crucial for supplying growing tumors with a vasculature to provide nutrients, oxygen, and remove waste products, as well as providing a conduit for the dispersal of metastases.^{10,11} The tissue localization of the VEGFRs and the tight control of angiogenesis makes VEGFR modulation an attractive approach to selectively inhibit tumor

* Corresponding author. Tel.: +1 318 342 1725; fax: +1 318 342 1737.

E-mail address: elsayed@ulm.edu (Khalid A. El Sayed).

growth and metastasis, without affecting the surrounding normal tissue.⁹ Although VEGF was initially thought to be an endothelial cell-specific growth factor, recent reports have identified VEGF receptors on non-endothelial cells.¹² Liang et al., for example, have shown that VEGF can induce proliferation and survival of breast cancer cells expressing VEGFR2 (flk) through the MAPK/ERK signaling pathway.¹² Targeting the VEGF receptor and/or its downstream signaling pathways would block the VEGF-dependent proliferation and angiogenesis of tumor cells.

The work presented herein shows the design and synthesis of dibromotyrosine analogues as anti-angiogenic agents and inhibitors of human prostate cancer proliferation, invasion, and migration with negligible cytotoxicity.

2. Results and discussion

Analogues were designed based on docking experiments at the ATP binding site of the vascular endothelial growth factor receptor 2 (VEGFR2). Two intermediates, **2** and **3**, from the synthetic scheme of verongiaquinol (Supplementary data, Scheme S1) were selected as starting scaffolds for the generation of new analogues. These simple dibrominated phenolic scaffolds are common in drug discovery programs. In fact, there is plenty of literature describing brominated phenolic and polyphenolic compounds as promising anti-cancer candidates currently under further development.^{13,14}

Two sets of reactions, guided by docking studies, were carried out (Schemes 1 and 2). The first reaction set included the esterification of the phenolic hydroxyl group with a variety of alkyl and aryl acid chlorides, using *N,N*-dimethylaminopyridine (DMAP) as a catalyst (Scheme 1).^{15,16} The other reaction set included the etherification of the same phenolic hydroxyl group using a variety of alkyl and aryl bromides in the presence of NaH (Scheme 2).^{16,18} Analogues were then screened for biological activity in the MTT, wound-healing and Cultrex[®] BME cell invasion assays against the

human prostate cancer cell line, PC-3 and for anti-angiogenic activity in the chick chorioallantoic membrane (CAM) assay. In general, ester analogues were more active as anti-migratory agents whereas ether analogues proved to be more active in the proliferation assay. Also, consistent with in silico data, those analogues with higher docking scores showed promising anti-angiogenic activity in the CAM assay. Unlike verongiaquinol, none of the analogues showed any evidence of cytotoxicity towards bone marrow myeloid progenitor cells (GM-CFC). The GM-CFC assay was conducted using a commercial colony forming assay (HALO[®] kit) to assess the cytotoxic potential of various analogues against a non-cancerous cell type often affected by cancer chemotherapeutics.

2.1. Chemistry

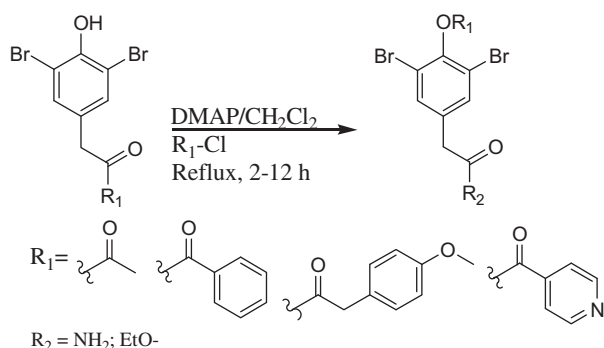
Six new and one known ester analogues (**4–10**) were synthesized via the DMAP-catalyzed nucleophilic addition reaction of **2** and **3** with alkyl, aryl and heterocyclic acid chlorides to generate the corresponding esters in 37–82% yields (Scheme 1).^{15,16}

The HREIMS of **4** showed an $[M+H]^+$ peak at m/z 349.9166, suggesting the molecular formula $C_{10}H_9Br_2NO_3$ and a possible C-1 acetyl ester analogue of **2**. Further investigation of ¹H and ¹³C NMR data proved that **4** is a known natural product that was previously isolated from the marine sponge *Suberea* aff. *Praetensa*.¹⁷

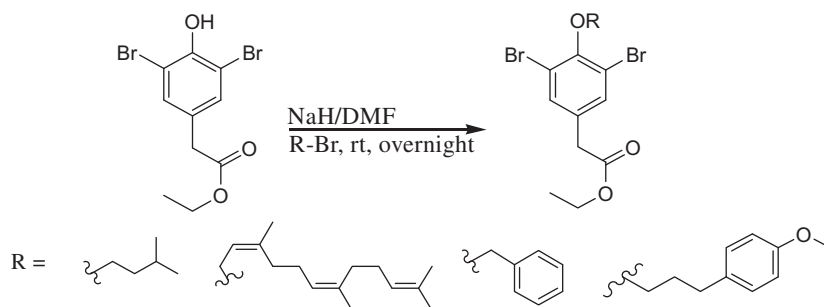
The HREIMS, ¹H and ¹³C NMR data of **5** (Tables 1 and 2) suggested the molecular formula $C_{15}H_{11}Br_2NO_3$ and possible C-1 benzoate ester analogue of **2**. The upfield shift of C-1 ($\Delta\delta$ –4.4) as well as the downfield shifts of C-4 ($\Delta\delta$ +6.0) and C-2/6 ($\Delta\delta$ +7.1), as compared to the parent **2** (Table S1), provided the evidence for C-1 benzylation. Furthermore, the aromatic methine doublet H-3' (δ_H 8.20) showed ³J-HMBC correlations with the quaternary carbonyl carbon C-1' (δ_C 163.6) and the aromatic carbon C-5' (δ_C 134.4), confirming the presence of an intact benzoyl moiety. Thus, compound **5** was determined to be 2,6-dibromo-1-benzoyloxybenzene-4-acetamide.

The HREIMS, ¹H and ¹³C NMR data of **6** (Tables 1 and 2) suggested the molecular formula $C_{17}H_{15}Br_2NO_3$ and possible C-1 2-(4-methoxyphenyl)acetic acid ester analogue of **2**. The methoxy protons singlet H_{3-1''} (δ_H 3.77) showed a ³J-HMBC correlation with the quaternary aromatic carbon C-6' (δ_C 159.1). The aromatic methine doublet H-4' (δ 7.29) showed ³J-HMBC correlations with C-6' and methylene carbon C-2' (δ_C 40.0). The methylene protons H_{2-2'} (δ_H 3.87) showed ³J-HMBC correlations with the quaternary carbonyl carbon C-1' (δ_C 168.7), the aromatic quaternary carbon C-3' (δ_C 124.6) and the aromatic methane carbons C-4'/8' (δ_C 130.8). Thus, compound **6** was determined to be 2,6-dibromo-1-(*p*-methoxyphenylacetoxyl)benzene-4-acetamide.

The HREIMS, ¹H and ¹³C NMR data of **7** (Tables 1 and 2) suggested the molecular formula $C_{12}H_{12}Br_2O_4$ and possible C-1 acetyl ester analogue of **3**. The ³J-HMBC correlation between the methyl protons H_{3-2'} (δ_H 2.38) and the quaternary carbonyl carbon C-1'



Scheme 1. General synthetic scheme for ester analogues **4–10**.



Scheme 2. General synthetic scheme of ether analogues **11–14**.

Table 1
¹H NMR Data of compounds **5–10**^a

Position	δ_{H}					
	5	6	7	8	9	10
3/5	7.51, s	7.44, s	7.49, s	7.55, s	7.46, s	7.56, s
7	3.48, s	3.44, s	3.54, s	3.58, s	3.53, s	3.59, s
9	—	—	4.16, q (7.0)	4.18, q (7.3)	4.15, q (7.0)	4.18, q (7.2)
10	—	—	1.26, dd (7.3)	1.28, dd (7.4)	1.25, dd (7.0)	1.28, dd (7.2)
1'	—	—	—	—	—	—
2'	—	3.87, s	2.38, s	—	3.89, s	—
3'	8.20, d (8.0)	—	—	8.25, dd (7.0, 1.4)	—	8.04, dd (5.9, 1.2)
4'	7.50, dd (7.7)	7.29, d (8.4)	—	7.54, dd (7.7, 1.5)	7.32, dd (8.8, 2.2)	8.89, dd (5.9, 1.2)
5'	7.64, dd (7.3)	6.86, d (8.8)	—	7.67, dd (7.7, 1.1)	6.89, dd (8.8, 2.2)	—
6'	7.50, dd (7.7)	—	—	7.54, dd (7.7, 1.5)	—	8.89, d (5.9)
7'	8.20, d (8.0)	6.86, d (8.8)	—	8.25, dd (7.0, 1.4)	6.89, dd (8.8, 2.2)	8.04, d (5.9)
8'	—	7.29, d (8.4)	—	—	7.32, dd (8.8, 2.2)	—
1''	—	3.77, s	—	—	3.80, s	—

^a In CDCl₃, 400 MHz. Coupling constants (*J*) are in Hertz.**Table 2**
¹³C NMR Data of compounds **5–10**^a

Position	δ_{C}					
	5	6	7	8	9	10
1	145.5, qC	145.3, qC	145.4, qC	145.6, qC	145.3, qC	145.0, qC
2/6	117.9, qC	117.8, qC	117.6, qC	117.8, qC	117.6, qC	117.4, qC
3/5	133.3, CH	133.3, CH	133.3, CH	133.3, CH	133.2, CH	133.4, CH
4	135.7, qC	135.6, CH	134.7, qC	134.8, qC	134.7, qC	135.3, qC
7	41.4, CH ₂	41.5, CH ₂	40.1, CH ₂	40.1, CH ₂	40.1, CH ₂	40.1, CH ₂
8	172.9, qC	172.5, qC	170.3, qC	170.4, qC	170.3, qC	170.2, qC
9	—	—	61.5, CH ₂	61.5, CH ₂	61.5, CH ₂	61.5, CH ₂
10	—	—	14.2, CH ₃	14.3, CH ₃	14.2, CH ₃	14.2, CH ₃
1'	163.6, qC	168.7, qC	167.4, qC	163.2, qC	168.2, qC	161.9, qC
2'	128.2, qC	40.0, CH ₂	20.6, CH ₃	128.4, qC	40.1, CH ₂	135.7, qC
3'	130.6, CH	124.6, qC	—	130.7, CH	124.8, qC	123.5, CH
4'	128.8, CH	130.8, CH	—	128.8, CH	130.9, CH	151.0, CH
5'	134.4, CH	114.1, CH	—	134.2, CH	114.1, CH	—
6'	128.8, CH	159.1, qC	—	128.8, CH	159.0, qC	151.0, CH
7'	130.6, CH	114.1, CH	—	130.7, CH	114.1, CH	123.5, CH
8'	—	130.8, CH	—	—	130.9, CH	—
9'	—	55.3, CH ₃	—	—	55.4, CH ₃	—

qC = quaternary, CH = methine, CH₂ = methylene, CH₃ = methyl carbons.^a In CDCl₃, 100 MHz. Carbon multiplicities were determined by APT experiments.

(δ_{C} 167.4) supported the presence of the acetate ester. Thus, compound **7** was determined to be 2,6-dibromo-1-acetoxybenzene-4-acetic acid ethyl ester.

The HREIMS, ¹H and ¹³C NMR data of **8** (Tables 1 and 2) suggested the molecular formula C₁₇H₁₄Br₂O₄ and possible C-1 benzoate ester analogue of **3**. The assignment of benzoate ester was based on HMBC data as previously described in **5**. Thus, compound **8** was determined to be 2,6-dibromo-1-benzoyloxybenzene-4-acetic acid ethyl ester.

The HREIMS, ¹H and ¹³C NMR data of **9** (Tables 1 and 2) suggested the molecular formula C₁₉H₁₈Br₂O₅ and possible C-1 6'-methoxyphenylmethyl ester analogue of **3**. HMBC further confirmed this assignment as previously described in **6**. Thus, **9** was determined to be 2,6-dibromo-1-(*p*-methoxyphenylacetoxy)benzene-4-acetic acid ethyl ester.

The HREIMS of **10** showed a molecular ion peak at *m/z* 441.9269 suggesting the molecular formula C₁₆H₁₃Br₂NO₄ and possible C-1 esterification of **3** with an isonicotinoyl moiety. The ¹H, ¹³C NMR, and HMBC data (Tables 1 and 2) were used to verify C-1 esterification. The aromatic methine doublet H-3'/7' (δ_{H} 8.04) showed a ³J-HMBC correlation with the quaternary carbonyl carbon C-1' (δ_{C} 161.9) as well as a COSY coupling with the H-4'/6' doublet (δ_{H}

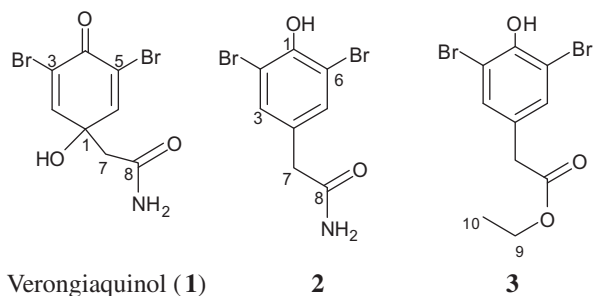
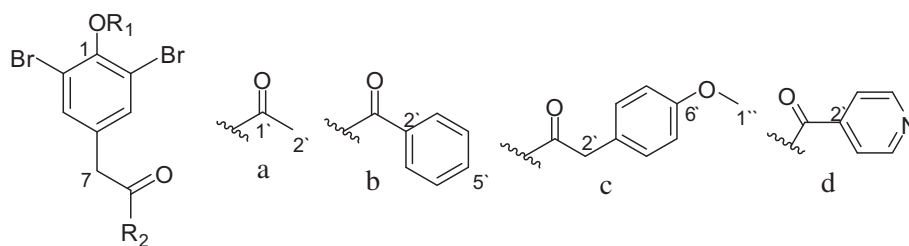
Table 3
¹H NMR Data of compounds **11–14**^a

Position	δ_{H}			
	11	12	13	14
3/5	7.43, s	7.47, s	7.42, s	7.42, s
7	3.51, s	3.53, s	3.51, s	3.50, s
9	4.16, q (7.0)	4.17, q (7.2)	4.16, q (7.2)	4.16, q (7.2)
10	1.26, t (7.2)	1.27, t (7.2)	1.26, t (7.2)	1.26, t (7.3)
1'	4.54, d (7.3)	5.01, s	4.01, t (6.4)	4.00, t (6.8)
2'	5.64, t (6.2)	—	2.15, m	1.75, q (13.6)
3'	—	7.60, m	2.83, t (7.9)	1.92, m
4'	2.10, m	7.37, m	—	0.98, d (6.6)
5'	2.15, m	7.42, m	7.17, d (8.8)	0.98, d (6.6)
6'	5.12, m	7.37, m	6.84, d (8.4)	—
7'	—	7.60, dd (6.6, 1.5)	—	—
8'	1.97, m	—	6.84, d (8.4)	—
9'	2.05, m	—	7.17, d (8.8)	—
10'	5.08, m	—	—	—
11'	—	—	3.79, s	—
12'	1.67, s	—	—	—
13'	1.74, s	—	—	—
14'	1.60, s	—	—	—
15'	1.59, s	—	—	—

^a In CDCl₃, 400 MHz. Coupling constants (*J*) are in Hertz.

8.89). Thus, **10** was determined to be 2,6-dibromo-1-(isonicotinoyloxy)benzene-4-acetic acid ethyl ester.

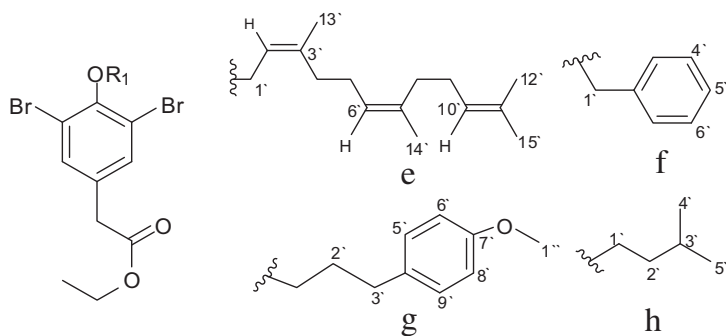
Analysis of ^1H and ^{13}C NMR data (Tables 3 and 4) showed that etherification primarily induced a downfield shift most signifi-

Verongiaquinol (**1**)**2****3**

	R ₁	R ₂
4	a	NH ₂
5	b	NH ₂
6	c	NH ₂
7	a	EtO
8	b	EtO
9	c	EtO
10	d	EtO

Four new ether analogues **11–14** were synthesized according to Scheme 2.¹⁸ This scheme shows the base-catalyzed nucleophilic substitution reaction¹⁶ in which the electrophilic center is the brominated carbon of the alkyl or alkenyl bromides used. Reaction yields ranged between 47% and 70%, with the aryl bromides giving the higher yields.

cantly at the C-1 and the C-2/6 positions. Carbon C-1 was shifted by $\Delta\delta +3.8$, while C-2/6 were shifted by $\Delta\delta +8.9$, as compared to the parent **3** (Table S1). The intact *trans, trans*-farnesyl moiety was confirmed by HMBC and ^1H - ^1H COSY experiments. The methylene proton doublet H₂-1' (δ_{H} 4.54) showed ^3J -HMBC correlations with the aromatic oxygenated quaternary carbon C-1 and



	R
11	e
12	f
13	g
14	h

The HREIMS data of **11** showed a molecular ion peak at m/z 581.0668, suggesting the molecular formula $\text{C}_{25}\text{H}_{34}\text{Br}_2\text{O}_3$ and possible C-1-etherification of **3** with a *trans, trans*-farnesyl moiety.

the quaternary olefinic carbon C-3' (δ_{C} 152.4 and 143.1, respectively). COSY correlations were observed between the olefinic methine H-2' (δ_{H} 5.64) and both H₂-1' and H₃-13' (δ_{H} 4.54 and

Table 4
¹³C NMR Data of compounds **11–14**^a

Position	δ_c			
	11	12	13	14
1	152.4, qC	152.0, qC	152.7, qC	152.7, qC
2/6	118.7, qC	118.5, qC	118.3, qC	118.4, qC
3/5	133.5, CH	133.6, CH	133.6, CH	133.5, CH
4	132.4, qC	132.9, qC	132.4, qC	132.4, qC
7	39.9, CH ₂	39.9, CH ₂	39.9, CH ₂	39.9, CH ₂
8	170.7, qC	170.6, qC	170.7, qC	170.7, qC
9	61.4, CH ₂	61.4, CH ₂	61.4, CH ₂	61.4, CH ₂
10	14.3, CH ₃	14.3, CH ₃	14.3, CH ₃	14.3, CH ₃
1'	70.1, CH ₂	74.7, CH ₂	73.0, CH ₂	72.2, CH ₂
2'	119.0, CH	136.3, qC	32.1, CH ₂	38.9, CH ₂
3'	143.1, qC	128.6, CH	31.4, CH ₂	24.9, CH
4'	39.7, CH ₂	128.6, CH	133.9, qC	22.8, CH ₃
5'	26.3, CH ₂	128.5, CH	129.5, CH	22.8, CH ₃
6'	123.8, CH	128.6, CH	113.9, CH	—
7'	135.5, qC	128.6, CH	157.9, qC	—
8'	39.8, CH ₂	—	113.9, CH	—
9'	26.8, CH ₂	—	129.5, CH	—
10'	124.4, CH	—	—	—
11'	131.4, qC	—	55.3, CH ₃	—
12'	25.8, CH ₃	—	—	—
13'	16.7, CH ₃	—	—	—
14'	16.1, CH ₃	—	—	—
15'	17.8, CH ₃	—	—	—

qC = quaternary, CH = methine, CH₂ = methylene, CH₃ = methyl carbons.^a In CDCl₃, 100 MHz. Carbon multiplicities were determined by APT experiments.

1.74, respectively). The olefinic proton H-6' (δ_H 5.12) showed COSY coupling with both methylene protons H₂-4' and H₂-5' (δ_H 2.10 and 2.15, respectively), and virtual coupling with the methyl H₃-14' (δ_H 1.60). The ³J-HMBC correlation between the methyl protons H₃-13' and C-4' (δ_c 39.7) connected both segments together. ¹H-¹H COSY and HMBC data further connected the rest of the farnesyl segment. Hence, **11** was determined to be 2,6-dibromo-1-(*trans, trans*-farnesyloxy) benzene-4-acetic acid ethyl ester.

The HREIMS, ¹H and ¹³C NMR data of **12** (Tables 3 and 4) suggested the molecular formula C₁₇H₁₆Br₂O₃ and possible C-1 benzyl ether analogue of **3**. The benzylic oxygenated methylene proton singlet H₂-1' (δ_H 5.01) showed ³J-HMBC correlations with the aromatic carbons C-1 and C-3'/C-7' (δ_c 152.0 and 128, respectively). Thus, **12** was determined to be 2,6-dibromo-1-(benzyloxy)-benzene-4-acetic acid ethyl ester.

Table 5

Docking scores for analogues **2–14** resulting from docking at the ATP binding site of VEGFR2 (PDB: 3cjf) using SYBYL 8.1 Surflex-Dock

Compound	Total score
Ligand	7.66
11	6.83
13	5.35
14	5.30
9	4.66
3	4.47
6	4.37
5	4.37
12	4.14
8	3.65
2	3.55
7	3.51
4	3.48
10	3.45
1	3.11

The HREIMS, ¹H and ¹³C NMR data of **13** (Tables 3 and 4) suggested the molecular formula C₂₀H₂₂Br₂O₄ and possible C-1 *p*-methoxyphenylpropyl ether analogue of **3**. The methylene proton triplet H₂-1' (δ_H 4.01) showed ³J-HMBC correlations with the oxygenated quaternary aromatic carbon C-1 and the aliphatic benzylic methylene carbon C-3' (δ_c 152.7 and 31.4, respectively). The methoxy protons singlet H₃-1'' (δ_H 3.79) showed a ³J-HMBC correlation with the oxygenated quaternary aromatic carbon C-7' (δ_c 157.9). The aromatic methine doublet H-5'/9' (δ_H 7.17) showed ³J-HMBC correlation with C-7' and C-3'. They also showed COSY coupling with the aromatic methine doublet H-6'/H-8' (δ_H 6.84). Thus, **13** was determined to be 2,6-dibromo-1-(*p*-methoxyphenylpropyl-oxy) benzene-4-acetic acid ethyl ester.

The HREIMS, ¹H and ¹³C NMR data of **14** (Tables 3 and 4) suggested the molecular formula C₁₅H₂₀Br₂O₃ and possible C-1 isopentyl ether analogue of **3**. The methylene proton triplet H₂-1' (δ_H 4.00) showed ³J-HMBC correlations with the oxygenated aromatic carbon C-1 and the aliphatic methine carbon C-3' (δ_c 152.7 and 24.9, respectively). The methyl proton doublet H₃-4'/H₃-5' (δ_H 0.98) showed COSY coupling with proton H-3' (δ_H 1.92), which was coupled to the methylene protons H₂-2' (δ_H 1.75). The latter also showed ¹H-¹H COSY coupling with H₂-1'. Thus, compound **14** was determined to be 2,6-dibromo-1-(3''-methylbutyloxy)benzene-4-acetic acid ethyl ester.

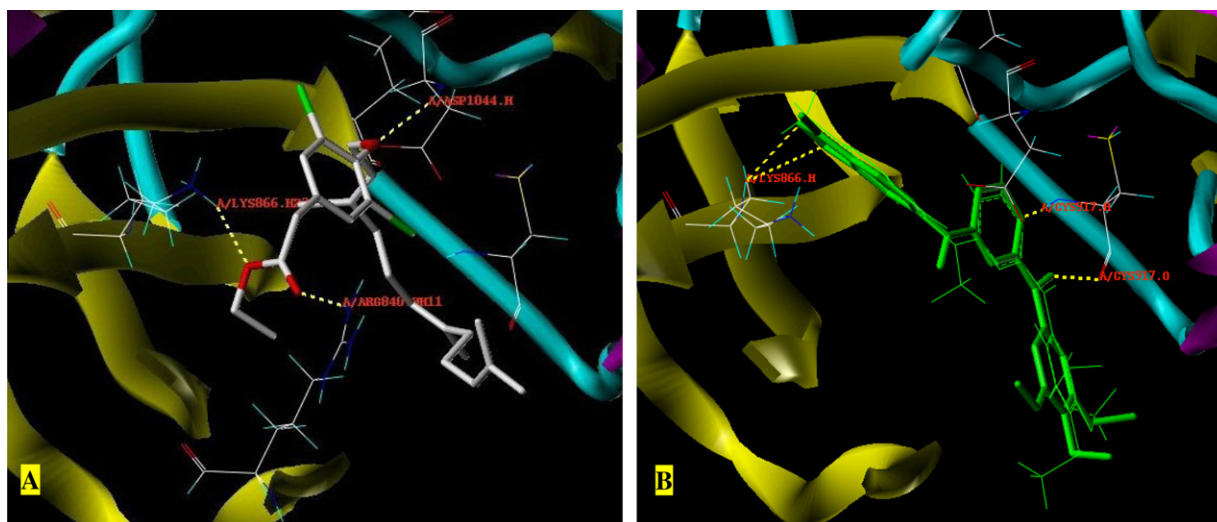


Figure 1. (A) Important HB interactions of **11** at the ATP binding site of VEGFR2 (PDB 3cjf). (B) Overlaid ligand obtained from the crystal structure of VEGFR2 (green stick) and the same ligand after the docking simulation (bold green).

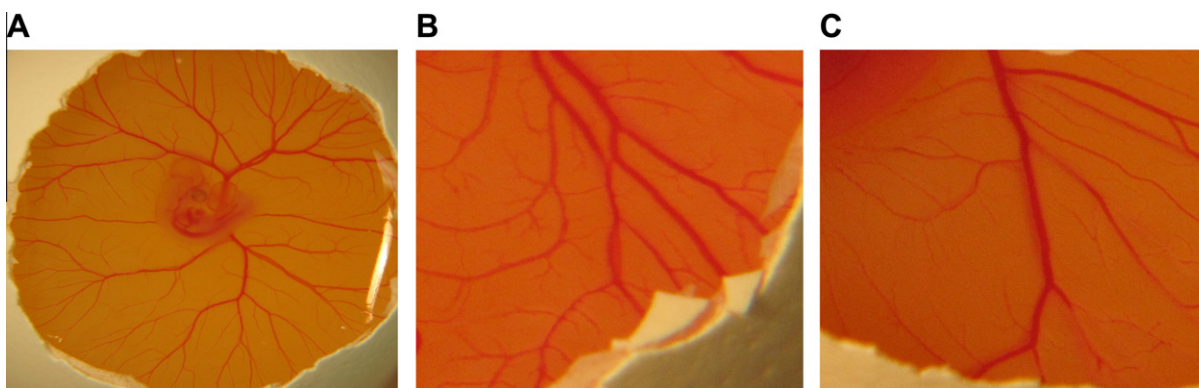


Figure 2. Chick chorioallantoic membrane (CAM) assay. (A) Growing vascular network at day-five prior to treatment. (B) Vascular network of a control-treated egg after 48 h (3×). (C) Vascular network of an egg treated with **13** (50 µg/disc) after 48 h (3×).

Table 6
Chick chorioallantoic membrane (CAM) assay results^a

Grade	Compounds
0	2, 3, 14
1	8, 9
2	4, 11, 13
3	5, 6, 10, 12

^a 0: Number of blood vessels per 48 mm² area around the treatment disc >16. 3: Number of blood vessels per 48 mm² area around the treatment disc <12.

Table 7
IC₅₀ Values of **2–14** using the MTT and WHA assays against PC-3 cells

Compound	MTT (IC ₅₀ , µM)	WHA (IC ₅₀ , µM)
2	>100	>100
3	>100	>100
4	>100	74.8
5	>100	12.2
6	>100	18.9
7	>100	>100
8	>100	44.6
9	>100	< 10
10	>100	44.6
11	16.5	19.9
12	29.7	75.5
13	40.0	57.9
14	49.2	91.3

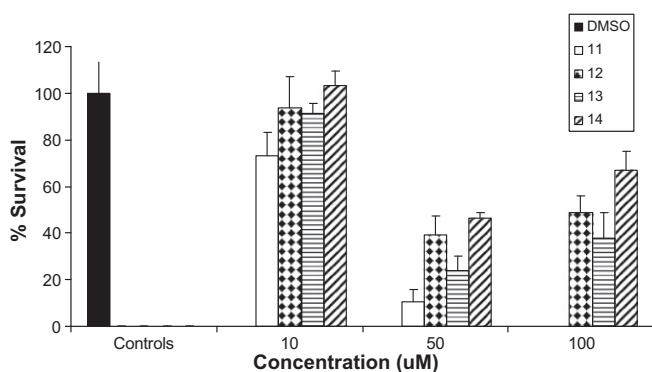


Figure 3. Anti-proliferative activity of ether analogues **11–14** against PC-3 cells. Error bars indicate the SD of $n = 3$ /dose.

2.2. Molecular docking studies

Analogues were docked into the ATP binding site of VEGFR2 (PDB code 3cjf) using Surflex-Dock interface implemented into SYBYL 8.0.^{19–21} Surflex-Dock is a fully automatic flexible molecular docking algorithm that combines the scoring function from the Hammerhead docking system with a search engine that relies on a surface-based molecular similarity method as a means to rapidly generate suitable putative poses for molecular fragments.^{19,20}

The high binding affinity of any active ligand with VEGFR2 is usually satisfied through hydrogen bonding (HB) interactions with the following amino acid residues: Lys866, Cys917, Asn921 and Asp1044.^{22–24} Compound **11** satisfied at least two of these interactions (Fig. 1A). Both ethyl ester oxygens are hydrogen bond acceptors (HBA) and are involved in reinforced ionic HB interactions with the positively charged guanidinium cation of Arg840 and protonated quaternary amino group of Lys866, respectively. Fur-

thermore, the ether oxygen is involved in a HB interaction with the amide NH of Asp1044. Table 5 shows the docking scores of analogues **1–14** versus the VEGFR2 ligand (*N*⁴-(3-methyl-1*H*-indazol-6-yl)-*N*²-(3,4,5-trimethoxyphenyl)-pyrimidine-2,4-diamine). The docking-scoring procedure was validated by docking the VEGFR2 ligand into the ATP binding site, resulting in a docked pose close to that observed in the crystallographic structure^{22,23} (Fig. 1B).

In an attempt to gain an insight into the effect of the type of the halogen at positions C-2 and C-6 on the biological activity, virtually designed difluoro and dichloro analogues of **2–14** were docked into the ATP binding site of VEGFR2 (Supplementary data, Table S3). Generally, with few exceptions, difluoro substitution proved associated with higher docking scores, which may imply superior activity versus the dibromo analogues. The difluoro substitution is uncommon in natural products and therefore the focus of this study remained on the dibromotyrosine analogues to mimic this common marine natural products class.

2.3. Biological activity

The anti-angiogenic potential of **4–14** was tested in the CAM assay. The anti-proliferative, anti-migratory and anti-invasive activities against the human prostate cancer cell line PC-3 were evaluated using the MTT, wound-healing and Cultrex[®] BME cell invasion assays, respectively.

2.3.1. Chick chorioallantoic membrane (CAM) assay

The chick chorioallantoic membrane (CAM) assay is a widely used in vivo model for the study of angiogenesis and represents a simple functional assay to screen agents for anti-angiogenic

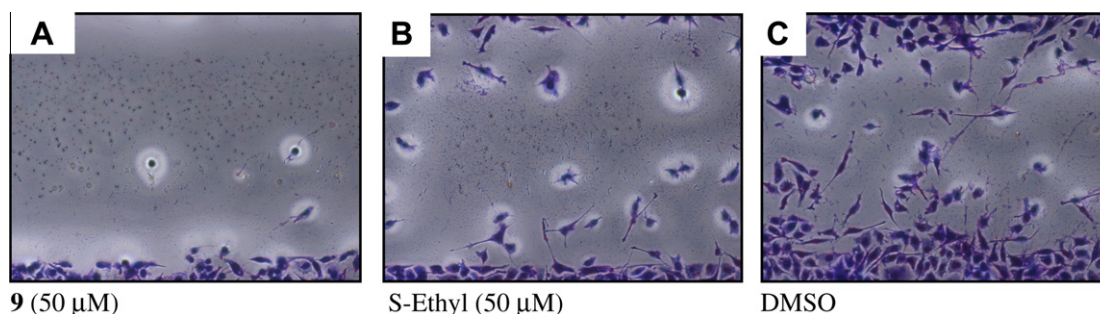


Figure 4. WHA using PC-3 cells after 24 h exposure to: (A) A 50 μM dose of **9**. (B) A 50 μM dose of (Z)-5-(4-(ethylthio)benzylidene)-hydantoin (S-Ethyl) as a positive control.³¹ (C) Vehicle (DMSO) treatment as a negative control.

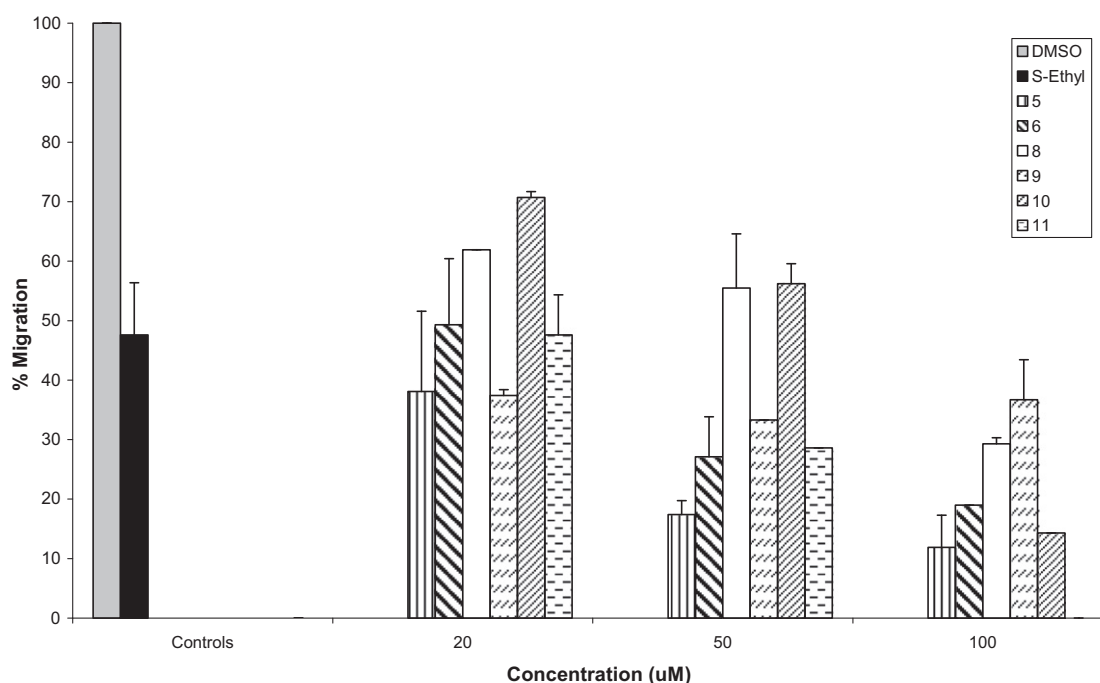


Figure 5. Anti-migratory activity of the most active analogues against the human prostate cancer cell line, PC-3. Error bars indicate the SD of $n = 3/\text{dose}$.

activity.²⁵ The main advantages of the CAM assay are its low-cost, simplicity, reliability, and applicability to large-scale screening.²⁶ VEGFR2 is expressed in CAM's endothelial cells and the pericytes, while VEGF is expressed in the chorionic epithelial cells.²⁵ VEGF release promotes angiogenesis via initiating endothelial cells expressing VEGFR2 in the CAM blood vessels.²⁵ Therefore, modulation of VEGFR2 will directly correlate with angiogenesis inhibition in the CAM model. Analogues **4–14** as well as the parent compounds **2** and **3** were tested at 1, 10, and 50 $\mu\text{g}/\text{disc}$ doses in this assay. Evaluation of the anti-angiogenic potential was based on two criteria; the number of newly formed blood vessels as well as the length of these blood vessels (Fig. 2). Analogues were then graded using a 0–3 scale,²⁶ 0 grade being inactive and 3 showing the highest activity. As predicted in silico (Table 5), analogues with docking scores higher than 4.0 showed good activities within grades 2 and 3 (Table 6), including the most active **5**, **6**, and **11–13**. The only outliers were compound **14** with a good docking score of 5.30 but no activity (grade 0), and compounds **4** and **10**, with low docking scores of 3.48 and 3.45, respectively, but showed good activity (grades 2 and 3, respectively). Such deviation could be attributed to the activity of **4**, **10**, and **14** on unknown protein target(s) other than VEGFR2.

2.3.2. MTT Assay

The MTT assay allows for the measurement of cell viability and proliferation of cell populations in a quantitative colorimetric fashion by utilizing cellular ability to reduce the MTT reagent to insoluble purple formazan dye.^{27–29} In this assay, each analogue was tested at three concentrations; 10, 50, and 100 μM (Fig. 3). The concentration of each analogue that resulted in 50% cell growth inhibition, IC_{50} , was measured (Table 7). All other analogues showed lower IC_{50} values than any of the ester analogues (Fig. 3). Consistent with in silico studies, the farnesyl analogue **11** showed the most potent inhibition with an IC_{50} value of 16.5 μM . A closer look at the structural features of the most active analogues suggests that chain extension and unsaturation, as in **11**, are associated with a better activity profile compared to those with shorter saturated chains, as in **14**. Electron donating substituents and longer chain linking the aromatic ring to the ether oxygen, as in **13**, afforded a better anti-proliferative activity profile versus the simple unsubstituted benzyl ether **12**.

2.3.3. Wound-healing assay (WHA)

The wound-healing assay is a simple method for the study of directional cell migration in vitro.^{30,31} Figure 4 shows cell migra-

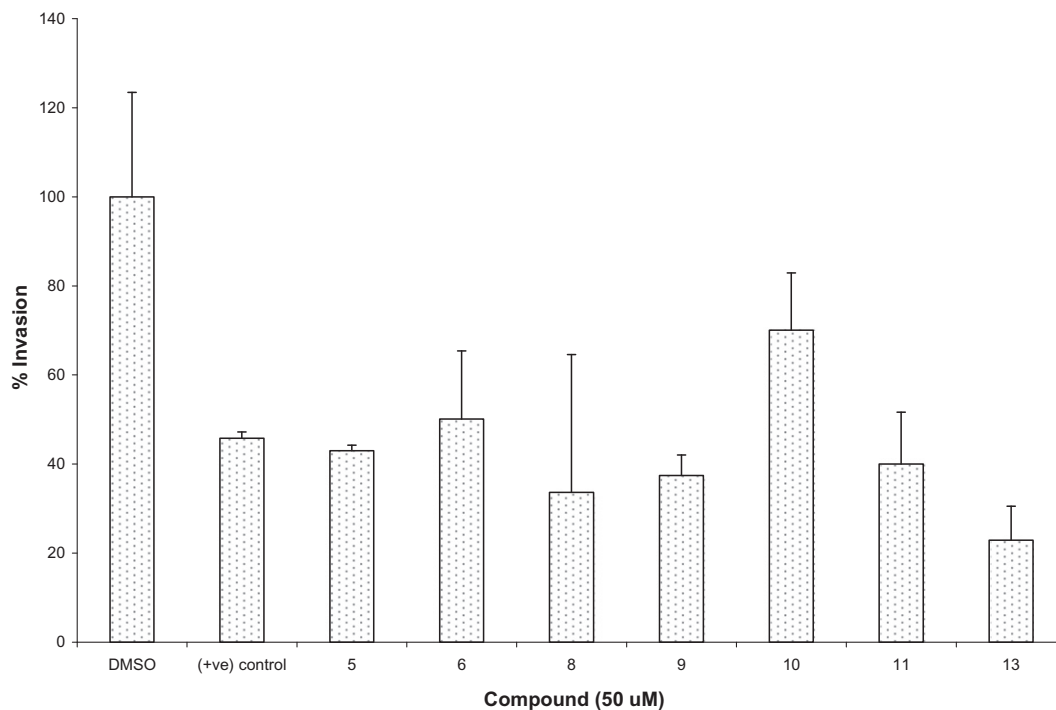


Figure 6. Anti-invasive activities of 50 μM dose of selected ester and ether analogues against the human prostate cancer cell line, PC-3 in the Cultrex[®] BME cell invasion assay kit. (Z)-5-(4-(ethylthio)benzylidene)imidazolidine-2,4-dione was used as a positive control.³¹ Error bars indicate the SD of $n = 3$ /analogue.

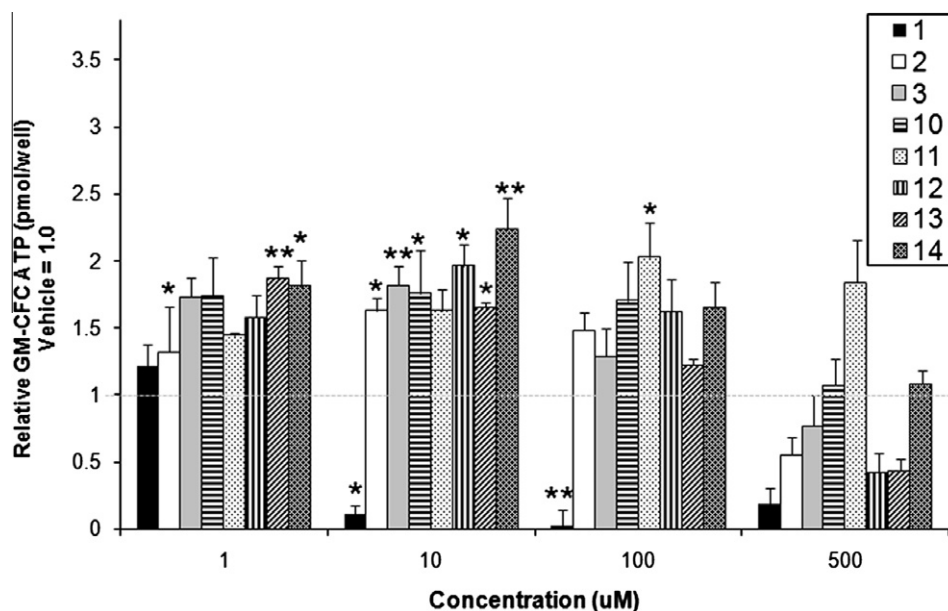


Figure 7. GM-CFC HALO[®] assay results. ATP luminescence for culture wells with compounds was normalized to mean of concurrent vehicle for each compound. Compounds were tested in two separate platings with vehicle means \pm SEM of 46.2 ± 3.9 (1, 10, and 11) and 113.0 ± 9.7 (2, 3, 12, 13, and 14) pmol/well. Relative treatment means \pm SEM ($n = 4$) are shown.

tion across the wound inflicted in the PC-3 cell monolayer for the vehicle and positive controls, and the active analogue **9**. The concentration of each analogue that results in 50% inhibition of cell migration, IC_{50} , was measured (Table 7). Interestingly, ester analogues showed a better anti-migratory profile than ether analogues, except for the farnesyl ether **11**. Figure 5 shows the anti-migratory effect of the most active analogues. Analogues **5**, **6**, and **9–11** showed a much better activity profile than the positive control, (Z)-5-(4-(ethylthio)benzylidene)-hydantoin used at a 50 μM dose (reported IC_{50} 51.4 μM).³¹ The amide or ethyl ester

side chains in compounds **4–6** and **7–10** had no observable influence on the activity pattern. In general, aromatic and heteroaromatic esters proved to be more active than aliphatic esters.

2.3.4. Cultrex[®] BME cell invasion assay

The Cultrex[®] BME cell invasion assay is an accelerated in vitro screening process for compounds that influence cell migration through extracellular matrices, which is a fundamental function of cellular processes such as angiogenesis, embryonic development, immune response, and metastasis of cancer cells.^{32,33} Those ester

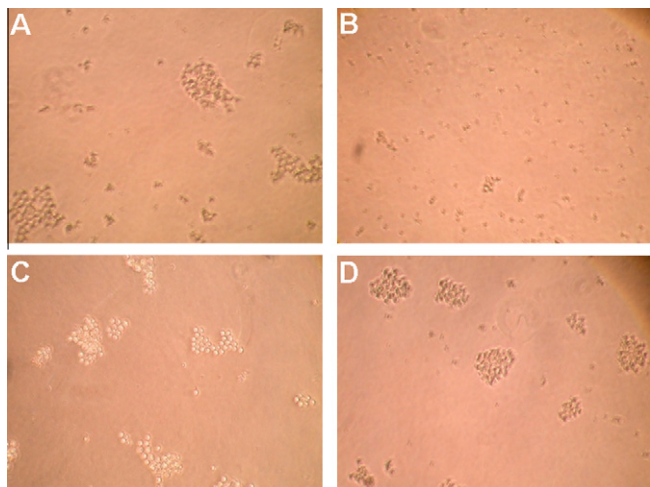


Figure 8. GM-CFC on the 3rd day after incubation with vehicle (A) and 10 μ M of **1** (B), **10** (C), and **11** (D).

analogues that showed the best IC_{50} values in the WHA (**5**, **6**, and **8–10**), as well as the two most active ether analogues (**11** and **13**) were tested at a single concentration of 50 μ M for their ability to inhibit the invasion of PC-3 cells (Fig. 6). Analogues showed a comparable activity profile to the known anti-invasive positive control, (Z)-5-(4-(ethylthio)benzylidene)-hydantoin,³¹ with compound **13** being almost twofold more active than this positive control.

2.3.5. GM-CFC/HALO[®] assay

The phenol structure, rather than the free radical-producing dienone observed in verongiaquinol, was selected as the starting point for the synthesis of all analogues as a strategy to eliminate the source of free radicals, thus eliminating the free radical-mediated cytotoxicity. A clonogenic assay for rat bone marrow myeloid progenitors (GM-CFC HALO[®] assay) was used as a model to test the cytotoxic potential of verongiaquinol and analogues. In this assay, the number of colonies formed in methylcellulose supplemented with myeloid growth/differentiation factors (GM-CSF, IL-3 and SCF) is monitored. Tested compounds **2–3**, **11**, and **13–14** showed no cytotoxic effects and no inhibition of colony formation even at 100 μ M, whereas verongiaquinol was cytotoxic at 10 μ M (Figs. 7 and 8). This clearly highlights the potential of dibromotyrosine analogues as effective and non-toxic hits because cells used in this assay are normal bone marrow cells. Therefore dibromotyrosines may have excellent therapeutic potential for the control of metastatic prostate cancer.

3. Conclusion

Structurally simple dibrominated phenolic compounds inspired by marine secondary metabolites offer interesting scaffolds for anti-cancer drug discovery. We showed herein the synthesis and biological evaluation of a series of ether and ester analogues of dibromotyrosine intermediates from the synthetic scheme of verongiaquinol. The results obtained demonstrate the potential of these dibrominated scaffolds as effective anti-angiogenic and inhibitors of prostate cancer proliferation and migration and are appropriate for further optimization.

4. Experimental

4.1. General experimental procedures

IR spectra were recorded on a Varian 800 FT-IR spectrophotometer. TLC analysis was carried on precoated Si Gel 60 F₂₅₄ 500 μ m

TLC plates (EMD Chemicals), using CHCl₃–MeOH (9.8:0.2) or (9:1) as developing systems. For column chromatography, Si Gel 60 (Natland International Corporation, 230–400 mm) was used, and gradient *n*-hexane–EtOAc or CHCl₃–MeOH solvent systems were used. HPLC analyses were conducted on a Shimadzu HPLC system (Columbia, MD) using a 5 μ m C18 column (150 \times 4.6 mm id; Agilent, Santa Clara, CA) and isocratic elution (CH₃OH/H₂O; 80:20) with UV detection set at 230 nm to verify the purity of compounds **4–14**. A purity of >95% was established for compounds **4–8**, **10** and **14** by HPLC analysis. Compounds **9** and **11–13** showed a purity of >90%. The ¹H and ¹³C NMR spectra were recorded in CDCl₃ and CD₃OD, using (CH₃)₄Si as an internal standard, on a JEOL Eclipse NMR spectrometer operating at 400 MHz for ¹H NMR and 100 MHz for ¹³C NMR. The HREIMS experiments were conducted at Louisiana State University on a 6200-TOF LC-MS (Agilent, Santa Clara, CA) equipped with a multimode source (mixed source that can ionize the samples alternatively by ESI and APCI).

4.2. Chemical reactions

4.2.1. Esterification of **2** and **3**

To solutions of **2** or **3** (0.148 mmol) in CH₂Cl₂ (5.0 mL), *N,N*-dimethylaminopyridine (2 equiv), and different alkyl or aryl acid chlorides (2 equiv) were added (Scheme 1).^{15,16} Each solution was separately stirred and refluxed (60–70 °C) for 2–12 h. Each reaction mixture was diluted with CH₂Cl₂, poured into water (10.0 mL), shaken and collected. Each CH₂Cl₂ layer was then shaken with 0.1 N HCl (2 \times 10.0 mL) and dried over anhydrous Mg₂SO₄. Crude mixtures were then purified on Si Gel 60 using gradient CHCl₃/MeOH system. Evaporation of fractions containing target compounds afforded **4–10** in 37–82% yields.

4.2.2. Etherification of **3**

Solutions of **3** (0.148 mmol) in dry DMF (1.0 mL) were added drop-wise to cooled (5 °C) oil-free suspension of NaH (0.148 mmol) in 1.0 mL dry DMF (Scheme 2). Different alkyl or aryl bromides (0.148 mmol) were then added drop-wise to the mixture.^{16,18} After H₂ evolution ceased, solutions were warmed to room temperature and stirred overnight. Each solution was then poured into 1 N NaOH and the mixture was extracted with CHCl₃ (3 \times 10 mL). Organic layer was then washed with brine (1 \times 10 mL) and dried over anhydrous Na₂SO₄. Crude mixtures were then purified on Si Gel 60 using gradient CHCl₃–MeOH or *n*-hexane–EtOAc systems, which afforded **11–14** in 47–70% yields.

4.2.3. 2,6-Dibromo-1-acetoxybenzene-4-acetamide (**4**)

A reaction of 50 mg of **2** with 23.2 μ L of acetyl chloride was carried out to give **4**, 47% yield: white powder; IR ν_{max} (CH₂Cl₂) 2987, 1772, 1693, 1653, 1208, 1182, 896 cm⁻¹; HRESIMS m/z 349.9166 [M+H]⁺ (calcd for C₁₀H₁₀Br₂NO₃, 349.9027).¹³

4.2.4. 2,6-Dibromo-1-benzoyloxybenzene-4-acetamide (**5**)

A reaction of 25 mg of **2** with 18.8 μ L of benzoyl chloride was carried out to give **5**, 72% yield: white powder; IR ν_{max} (CH₂Cl₂) 2987, 1749, 1695, 1557, 1235, 896 cm⁻¹; ¹H and ¹³C NMR, see Tables 3 and 4; HRESIMS m/z 413.9196 [M+3H]³⁺ (calcd for C₁₅H₁₄Br₂NO₃, 413.9340).

4.2.5. 2,6-Dibromo-1-(*p*-methoxyphenylacetoxy)benzene-4-acetamide (**6**)

A reaction of 25 mg of **2** with 24.8 μ L of 4-methoxyphenylacetyl chloride was carried out to give **6**, 59% yield: white powder; IR ν_{max} (CH₂Cl₂) 2987, 1770, 1695, 1248, 1155, 987 cm⁻¹; ¹H and ¹³C NMR, see Tables 3 and 4; HRESIMS m/z 457.9432 [M+3H]³⁺ (calcd for C₁₇H₁₈Br₂NO₄, 457.9602).

4.2.6. 2,6-Dibromo-1-acetoxybenzene-4-acetic acid ethyl ester (7)

A reaction of 50 mg of **3** with 21.0 μL of acetyl chloride was carried out to give **7**, 58% yield: clear oil; IR ν_{max} (CH_2Cl_2) 2987, 1773, 1734, 1557, 1181, 896 cm^{-1} ; ^1H and ^{13}C NMR, see Tables 3 and 4; HRESIMS m/z 380.9270 $[\text{M}+3\text{H}]^{3+}$ (calcd for $\text{C}_{12}\text{H}_{15}\text{Br}_2\text{O}_4$, 380.9336).

4.2.7. 2,6-Dibromo-1-benzoyloxybenzene-4-acetic acid ethyl ester (8)

A reaction of 50 mg of **3** with 17.2 μL of benzoyl chloride was carried out to give **8**, 37% yield: clear oil; IR ν_{max} (CH_2Cl_2) 2987, 1773, 1734, 1421, 1181, 896 cm^{-1} ; ^1H and ^{13}C NMR, see Tables 3 and 4; HRESIMS m/z 450.8912 $[\text{M}-\text{C}_2\text{H}_4+\text{K}]^+$ (calcd for $\text{C}_{15}\text{H}_{10}\text{Br}_2\text{O}_4\text{K}$, 450.8583).

4.2.8. 2,6-Dibromo-1-(*p*-methoxyphenylacetoxy)benzene-4-acetic acid ethyl ester (9)

A reaction of 50 mg of **3** with 22.6 μL of 4-methoxyphenylacetyl chloride was carried out to give **9**, 82% yield: yellow oil; IR ν_{max} (CH_2Cl_2) 2987, 1769, 1734, 1551, 1272, 896 cm^{-1} ; ^1H and ^{13}C NMR (Tables 3 and 4); HRESIMS m/z 484.9412 $[\text{M}+\text{H}]^+$ (calcd for $\text{C}_{19}\text{H}_{19}\text{Br}_2\text{O}_5$, 484.9599).

4.2.9. 2,6-Dibromo-1-(isonicotinoyloxy)benzene-4-acetic acid ethyl ester (10)

A reaction of 50 mg of **3** with 26.3 mg of isonicotinoyl chloride hydrochloride, in the presence of 62 μL Et_3N and 18.0 mg (1 equiv) DMAP, was carried out to give **10**, 86% yield: clear oil; IR ν_{max} (CHCl_3) 2991, 1760, 1732, 1644, 1140, 891 cm^{-1} ; ^1H and ^{13}C NMR, see Tables 3 and 4; HRESIMS m/z 441.9269 $[\text{M}+\text{H}]^+$ (calcd for $\text{C}_{16}\text{H}_{14}\text{Br}_2\text{NO}_4$, 441.9289).

4.2.10. 2,6-Dibromo-1-(*trans, trans*-farnesyloxy)benzene-4-acetic acid ethyl ester (11)

A reaction of 50 mg of **3** with 40.1 μL *trans, trans*-farnesyl bromide was carried out to give **11**, 86% yield: yellow oil; IR ν_{max} (CHCl_3) 2928, 1732, 1545, 1456, 948, 869 cm^{-1} ; ^1H and ^{13}C NMR, see Tables 5 and 6; HRESIMS m/z 581.0649 $[\text{M}+2\text{H}+\text{K}]^{3+}$ (calcd for $\text{C}_{25}\text{H}_{36}\text{Br}_2\text{O}_3\text{K}$, 581.0668).

4.2.11. 2,6-Dibromo-1-(benzyloxy)benzene-4-acetic acid ethyl ester (12)

A reaction of 50 mg of **3** with 17.6 μL benzyl bromide was carried out to give **12**, 50% yield: clear oil, IR ν_{max} (CHCl_3) 2928, 1732, 1546, 1260, 967, 857 cm^{-1} ; ^1H and ^{13}C NMR, see Tables 5 and 6; HRESIMS m/z 448.9266 $[\text{M}+\text{Na}]^+$ (calcd for $\text{C}_{17}\text{H}_{16}\text{Br}_2\text{O}_3\text{Na}$, 448.9364).

4.2.12. 2,6-Dibromo-1-(*p*-methoxyphenylpropyloxy)benzene-4-acetic acid ethyl ester (13)

A reaction of 50 mg of **3** with 25.9 μL 4-methoxyphenylpropyl bromide was carried out to give **13**, 51% yield: clear oil, IR ν_{max} (CHCl_3) 2938, 1733, 1612, 1545, 984, 842 cm^{-1} ; ^1H and ^{13}C NMR, see Tables 5 and 6; HRESIMS m/z 506.9587 $[\text{M}+\text{Na}]^+$ (calcd for $\text{C}_{20}\text{H}_{22}\text{Br}_2\text{O}_4\text{Na}$, 506.9783).

4.2.13. 2,6-Dibromo-1-(3'-methylbutyloxy)phenylacetic acid ethyl ester (14)

A reaction of 50 mg of **3** with 17.72 μL 3-methylbutyl bromide was carried out to give **14**, 47% yield: clear oil; IR ν_{max} (CHCl_3) 2957, 1733, 1545, 1457, 978, 872 cm^{-1} ; ^1H and ^{13}C NMR, see Tables 5 and 6; HRESIMS m/z 428.9676 $[\text{M}+\text{Na}]^+$ (calcd for $\text{C}_{15}\text{H}_{20}\text{Br}_2\text{O}_3\text{Na}$, 428.9677).

4.3. Molecular modeling

Three-dimensional structure building and all modeling were performed using the SYBYL program package, version 8.0, installed

on DELL desktop workstations equipped with a dual 2.0 GHz Intel® Xeon® processor running the Red Hat Enterprise Linux (version 5) operating system.³⁴ Conformations of each compound were generated using Confort™ conformational analysis. Energy minimizations were performed using the Tripos force field with a distance-dependent dielectric and the Powell conjugate gradient algorithm with a convergence criterion of 0.01 kcal/(mol Å).³⁵ Partial atomic charges were calculated using the semi-empirical program MOPAC 6.0 and applying the AM1.³⁶

4.3.1. Molecular docking

Surfex-Dock Program version 2.0 interfaced with SYBYL 8.0 was used to dock the compounds in the ATP binding site of VEGFR2.³⁷ Surfex-Dock employs an idealized active site ligand (protomol) as a target to generate putative poses of molecules or molecular fragments. These putative poses were scored using the Hammerhead scoring function.^{38,39} The 3D structure was taken from the Brookhaven Protein Databank (PDB code: 3cjf).²³

4.4. Cell culture

Prostate cancer cell line, PC-3 was purchased from ATCC (Manassas, VA). The cell line was grown in RPMI 1640 medium (GIBCO-Invitrogen, NY) with 10% fetal bovine serum (FBS) and supplemented with glutamine (2 mmol/L), penicillin G (100 $\mu\text{g}/\text{mL}$), and streptomycin (100 $\mu\text{g}/\text{mL}$) at 37 °C under 5% CO_2 .

4.4.1. Preparation of various dilutions of analogues for cell culture assays

A stock solution of each analogue was prepared by dissolving the compound in DMSO at a concentration of 50 mM for all assays. About 2 μL of each stock solution was transferred to 998 μL of serum-free medium to obtain 100 μM concentrations (0.2% DMSO). Serial dilutions were then conducted to obtain the desired concentrations for each assay. The negative control was prepared as follows: adding 2 μL DMSO to 998 μL serum-free media (MTT assay); adding 3 μL DMSO to 1497 μL serum-free media (WHA); adding 1.2 μL DMSO to 199 μL serum-free media (cell invasion assay).

4.5. MTT proliferation assay

The anti-proliferative effect of analogues was tested in culture on the human prostate cancer cell line, PC-3. Cell growth was measured using MTT kit (TACS™, Trevigen®, Inc.).^{27–29} Cells in exponential growth were plated in a 96-well plate at a density of 8×10^3 cells per well, and allowed to attach for 24 h at 37 °C under 5% CO_2 . Complete growth medium was then replaced with 100 μL of RPMI serum-free medium (GIBCO-Invitrogen, NY) containing various doses (10, 50, and 100 μM) of the specific test compound and incubation resumed at 37 °C under 5% CO_2 for 72 h. The cells were then treated with MTT solution (20 $\mu\text{L}/\text{well}$) and re-incubated for 4 h. The color reaction was stopped by the addition of solubilization/stop solution (100 $\mu\text{L}/\text{well}$), and incubation at 37 °C was continued to ensure complete dissolution of the formazan product. Absorbance of the samples was determined at λ 570 nm with an ELISA plate reader (BioTek, VT, USA). The IC_{50} value for each compound was calculated by nonlinear regression (curve fit) of log (concentration) versus the % survival, implemented in GraphPad Prism version 5.0 (GraphPad Software, La Jolla, CA, USA). The % cell survival was calculated as follows: % cell survival = $(\text{Abs}_{\text{treatment}}/\text{Abs}_{\text{DMSO}}) * 100\%$.

4.6. Wound-healing assay^{30,31}

PC-3 cells were plated onto sterile 24-well plates and allowed to form a confluent cell monolayer per well (>95% confluence) over-

night. Wounds were then inflicted in each cell monolayer using a sterile 200 μL pipette tip. Media was removed and cells were washed twice with PBS and once with fresh serum-free media. Test compounds at the desired concentrations (20, 50, and 100 μM) in fresh serum-free media were added to each well. The incubation was carried out for 24 h under serum-free conditions, after which media was removed and cells were washed, fixed and stained using Diff-Quick™ staining (Dade Behring Diagnostics, Aguada, Puerto Rico). Cells which migrated across the inflicted wound were counted under the microscope in three or more randomly selected fields (magnification: 400 \times).

4.7. Cultrex® BME cell invasion assay

Anti-invasive activities were measured using Trevigen's Cultrex® BME cell invasion assay.³² About 50 μL of basement membrane extract (BME) coat was added per well of the top chamber. After an overnight incubation at 37 °C in a 5% CO₂ atmosphere, 50,000 PC-3 cells per 50 μL serum-free RPMI medium were added per well of the top chamber. 150 μL of RPMI medium was then added to the lower chamber. Media contained 10% FBS and penicillin/streptomycin as well as fibronectin (1 $\mu\text{L}/\text{mL}$) and *N*-formyl-Met-Leu-Phe (10 nM) as chemoattractants. Test compounds were prepared at 6 \times the desired concentration (300 μM) and 10 μL of each of the compounds was added per well of the top chamber. Cells were incubated at 37 °C under 5% CO₂ which allowed for cell migration from the top to the lower chamber. After 24 h, the top and bottom chambers were aspirated and washed with washing buffer supplied within the kit. About 100 μL of 1 \times cell dissociation solution/calcein-AM solution was added to the bottom chamber and incubated at 37 °C under 5% CO₂ for 1 h. The cells internalize calcein-AM, and the intracellular esterases cleave the AM moiety to generate free calcein. Fluorescence of the samples was determined at λ_{ex} 485 and λ_{em} 520 nm, with an ELISA plate reader (Bio-Tek, VT, USA). The number of cells that invaded through the BME coat was calculated by a standard curve.

4.8. Chick chorioallantoic membrane (CAM) assay

Fertilized hens' eggs (Flock # T18) obtained from Charles River Laboratories (Franklin Commons, CT, USA) were incubated at 37 °C and constant humidity for three days. Eggs were kept at a 45° angle and turned every 2–4 h as per provider's recommendations. On day four, a small hole was made in the shell at the pointed end of the egg. Using a 5-mL syringe fitted with an 18G needle, 2–3 mL of albumin was removed.^{26,40} This step aims at detaching the CAM from the shell.⁴⁰ The hole was then sealed with adhesive tape²⁵ and a window was created at the blunt end of the egg. The window was covered with transparent tape and the eggs were incubated in upright position with the window uppermost.⁴⁰ Tested compounds dissolved in CH₂Cl₂ or MeOH were loaded onto 2-mm diameter cellulose nitrate discs (Whatman, VWR) at different concentrations (1, 10 and 50 $\mu\text{g}/\text{disc}$).⁴¹ On day five, loaded discs were placed on the CAM, preferably on a sparsely vascularized area between two large blood vessels.⁴⁰ The eggs were then re-incubated. Images of the control and treated areas were captured at 0 time and every 6 h for 48 h. The anti-angiogenic activity of each tested compound was evaluated by counting the number of blood vessels per specified area around the treatment disc (8.0 \times 6.0 mm) as well as the change in the length of blood vessels observed at the end of the incubation time.

4.9. GM-CFC HALO® Assay

Bone marrow was flushed from rat femurs and mononuclear cells were isolated by centrifugation (400g, 30 min) through a

Histopaque-1077 density gradient. Cells were collected at the interface, washed and centrifuged (400g, 10 min), and resuspended in 0.25 mL of medium and counted using hemocytometer. The GM-CFC 2 assay was performed using a HALO kit as per supplier's instructions (HemoGenix, Colorado Springs, CO). In brief, 20,000 mononuclear cells in 15 μL medium were mixed with 60 μL methyl cellulose, 60 μL FCS, 15 μL growth factor mix (rat recombinant GM-CSF, IL-3 and SCF) and plated in 96-well plates. After 5 days, GM-CFC colonies were measured as ATP luminescence measured with luciferase and luciferin. ATP luminescence was calibrated against a standard curve generated on the same day. Dose means for all compounds were statistically compared to vehicle with two-way ANOVA with Bonferroni post-hoc pairwise comparisons.

Supplementary data

Supplementary data (structures of the known bromotyrosine-derived marine natural products listed in the article (Fig. S1), ¹H and ¹³C NMR data of **2** and **3**, LRMS Data of **1–3**, and Docking scores of **2–14** and their virtual difluoro and dichloro analogues at the ATP binding site of VEGFR2 (Tables S1–S3) as well as the verongiaquinol synthetic scheme (Scheme 1)) associated with this article can be found, in the online version, at doi:10.1016/j.bmc.2010.08.057.

References and notes

- Debitus, C.; Guella, G.; Mancini, I.; Waikredre, J.; Guemas, J. P.; Nicolas, J. L.; Pietra, F. *J. Mar. Biotechnol.* **1998**, *6*, 136.
- Koulman, A.; Proksch, P.; Eberl, R.; Beekman, A. C.; Uden, W.; Konings, A. W. T.; Pedersen, J. A.; Pras, N.; Woerdenbag, H. J. *J. Nat. Prod.* **1996**, *59*, 591.
- Ankudey, F. J.; Kiprof, P.; Stromquist, E. R.; Chang, L. C. *Planta Med.* **2008**, *74*, 555.
- Teeyapant, R.; Kreis, P.; Wray, V.; Witte, L.; Proksch, P. *Z. Naturforsch.* **1993**, *48c*, 640.
- D'Ambrosio, M.; Guerriero, A.; Pietra, F. *Helv. Chim. Acta* **1984**, *67*, 1484.
- Cordoba, R.; Salvador Tormo, N.; Fernandez Medarde, A.; Plumet, J. *Bioorg. Med. Chem.* **2007**, *15*, 5300.
- Kreuter, M. H.; Leake, R. E.; Rinaldi, F.; Müller-Klieser, W.; Maidhof, A.; Müller, W. E. G.; Schröder, H. C. *Comp. Biochem. Physiol.* **1990**, *97B*, 151.
- Rodríguez-Nieto, S.; González-Iriarte, M.; Carmona, R.; Muñoz-Chápuli, R.; Medina, M. A.; Quesada, A. R. *FASEB J.* **2002**, *16*, 261.
- Manley, P. W.; Furet, P.; Bold, G.; Brügggen, J.; Mestan, J.; Meyer, T.; Schnell, C. R.; Wood, J. J. *Med. Chem.* **2002**, *45*, 5687.
- Kerbel, R. S. *Carcinogenesis* **2000**, *21*, 505.
- McDonnell, C. O.; Hill, A. D.; McNamara, D. A.; Walsh, T. N.; Bouchier Hayes, D. *J. Eur. J. Surg. Oncol.* **2000**, *26*, 105.
- Liang, Y.; Brekken, R. A.; Hyder, S. M. *Endocr. Relat. Cancer* **2006**, *13*, 905.
- Uckun, F. M.; Dibirdik, I.; Qazi, S.; Vassilev, A.; Ma, H.; Mao, C.; Benyumov, A.; Emami, K. H. *Bioorg. Med. Chem.* **2007**, *15*, 800.
- Calcul, L.; Chow, R.; Oliver, A. G.; Tenney, K.; White, K. N.; Wood, A. W.; Fiorilla, C.; Crews, P. *J. Nat. Prod.* **2009**, *72*, 443.
- El Sayed, K. A.; Yousaf, M.; Hamann, M. T.; Avery, M. A.; Kelly, M.; Wipf, P. *J. Nat. Prod.* **2002**, *65*, 1547.
- Miller, A.; Solomon, P. H. *Writing Reaction Mechanisms in Organic Chemistry*; Harcourt Academic Press: California, USA, 1999.
- Kijjoo, A.; Watanadilok, R.; Sonchaeng, P.; Sawangwong, P.; Pedro, M.; Nascimento, M. S. J.; Silva, A. M. S.; Eaton, G.; Herz, W. *Z. Naturforsch., C: J. Biosci.* **2002**, *57*, 732.
- Pearce, B. C.; Parker, R. A.; Deason, M. E.; Qureshi, A. A.; Wright, J. J. *K. J. Med. Chem.* **1992**, *35*, 3595.
- Hoshi, M.; Takashima, A.; Noguchi, K.; Murayama, M.; Sato, M.; Kondo, S.; Saitoh, Y.; Ishiguro, K.; Hoshino, T.; Imahori, K. *Proc. Natl. Acad. Sci. U.S.A.* **1996**, *93*, 2719.
- MacAulay, K.; Woodgett, J. R. *Expert Opin. Ther. Targets* **2008**, *12*, 1265.
- Liu, S.; Shen, Z. *Yaoyue Xuebao* **2007**, *42*, 1227.
- Harris, P.; Boloor, A.; Cheung, M.; Kumar, R.; Crosby, R. M.; Davis-Ward, R. G.; Epperly, A. H.; Hinkle, K. W.; Hunter, R. N.; Johnson, J. H.; Knick, V. B.; Laudeman, C. P.; Luttrell, D. K.; Mook, R. A.; Nolte, R. T.; Rudolph, S. K.; Szcwzyk, J. R.; Truesdale, A. T.; Veal, J. M.; Wang, L.; Stafford, J. A. *J. Med. Chem.* **2008**, *51*, 4632.
- Harris, P.; Cheung, M.; Hunter, R. N.; Brown, M. L.; Veal, J. M.; Nolte, R. T.; Wang, L.; Liu, W.; Crosby, R. M.; Johnson, J. H.; Epperly, A. H.; Kumar, R.; Luttrell, D. K.; Stafford, J. A. *J. Med. Chem.* **2005**, *48*, 1610.
- Hilberg, F.; Roth, G. J.; Krssak, M.; Kautschitsch, S.; Sommergruber, W.; Tontsch-Grunt, U.; Garin-Chesa, P.; Bader, G.; Zoepfel, A.; Quant, J.; Heckel, A.; Rettig, W. *J. Cancer Res.* **2008**, *68*, 4774.

25. (a) Peifer, C.; Dannhardt, G. *Anticancer Res.* **2004**, *24*, 1545; (b) Ribatti, D.; Cruz, A.; Nico, B.; Favier, J.; Vacca, A.; Corsi, P.; Roncali, L.; Dammacco, F. *Cytokine* **2002**, *17*, 262.
26. Ribatti, D.; Vacca, A.; Roncali, L.; Dammacco, F. *Curr. Pharm. Biotech.* **2000**, *1*, 73.
27. TACS™ MTT Cell Proliferation Assays Protocol, TREVIGEN® (www.trevigen.com, accessed on 05/27/2010).
28. Mosmann, T. J. *Immunol. Methods* **1983**, *65*, 55.
29. Alley, M. C.; Saudiero, D. A.; Monks, A.; Hursey, M. L.; Czerwinski, M. J.; Fine, D. L.; Abbott, B. J.; Mayo, J. G.; Shoemaker, R. H.; Boyd, M. R. *Cancer Res.* **1988**, *48*, 589.
30. Rodriguez, L. G.; Wu, X.; Guan, J. L. *Methods Mol. Biol.* **2005**, *294*, 23.
31. Mudit, M.; Khanfar, M.; Muralidharan, A.; Thomas, S.; Van Shah, G.; Soest, R. W. M.; El Sayed, K. A. *Bioorg. Med. Chem.* **2009**, *17*, 1731.
32. Cultrex® BME Cell Invasion Assay Protocol; www.trevigen.com, accessed on 05/27/2010.
33. Khanfar, M. A.; Youssef, D. T. A.; El Sayed, K. A. *ChemMedChem* **2010**, *5*, 274.
34. Khanfar, M. A.; Abu Asal, B.; Mudit, M.; Kaddoumi, A.; El Sayed, K. A. *Bioorg. Med. Chem.* **2009**, *17*, 6032.
35. Clark, M.; Cramer, R. D., III; van Opdenbosch, N. J. *Comput. Chem.* **1989**, *10*, 982.
36. Stewart, J. J. J. *Comput. Aided Mol. Des.* **1990**, *4*, 1.
37. Tripos Associates. SYBYL Molecular Modeling Software, version 8.0; Tripos Associates: St. Louis, MO, 2007; <http://www.tripos.com>, accessed on 05/27/2010.
38. Welch, W.; Ruppert, J.; Jain, A. N. *Chem. Biol.* **1996**, *3*, 449.
39. Ruppert, J.; Welch, W.; Jain, A. N. *Protein Sci.* **1997**, *6*, 524.
40. Murray, J. C. *Methods in Molecular Medicine*. In *Angiogenesis Protocols*; Humana Press Inc: Totowa, New Jersey, USA, 2001; Vol. 46.
41. Jain, S.; Shirode, A.; Yacoub; Shenouda; Barbo, A.; Sylvester, P. W.; Huntimer, E.; Halaweish, F.; El Sayed, K. A. *Planta Med.* **2007**, *73*, 591.